This is a repository copy of *Notch failure versus interior failure for mixed-mode in-plane loading*.

Notch failure versus interior failure for mixed-mode in-plane loading

Wenchao Li [a,*], Harm Askes [b], Luca Susmel [b]

[a] School of Civil Engineering, Chang'an University, Xi'an 710061,China

[b] Department of Civil and Structural Engineering, The University of Sheffield, Mappin Street, Sheffield S1 3JD, United Kingdom

*Corresponding Author: Dr. **Wenchao Li**

School of Civil Engineering

Chang'an University, Xi'an, Shaanxi Province, 710061,China

Telephone: +86 13709147632

E-mail: wenchaoli@chd.edu.cn

Abstract: This paper uses the linear-elastic Theory of Critical Distances (TCD) to verify and quantify the analysis of a particular central fracture mode occurring in the classical double-cracked flat plate specimen subjected to mixed mode I / mode II loading. Analytical formulae for estimating the critical loading condition for such a special central fracture mode of double-cracked flat plate specimen are derived using both standard elastic beam theory and the TCD. The influence of the crack length, specimen geometry and material parameters on the critical loading angle for such a special central fracture mode is discussed in detail. Finally, in order to verify the proposed central fracture prediction formulae, linear elastic stress analyses for two double-cracked flat plate specimens made of different materials and having different loading angles were conducted using finite element analysis. The results in this study confirm the possibility of interior fracture modes and provide insight on the mechanism of analogous interior fracture occurring in practical applications.

Keywords: crack; analytical solutions; double-cracked flat plate specimen; central fracture mode; the Theory of Critical Distances

1. Introduction

Assessing the integrity of cracked-bodies continues to be a significant issue in the fracture community. It is generally accepted that the fracture of most cracked-components typically initiates from the crack tip due to the obvious localized stress concentration phenomenon. However, many investigations and practical failure analyses (e.g. Li et al., 2016; Taylor, 2011) show that not all of the practical components containing stress raisers fail at the stress raiser tip. For some cracked-components with a given geometry and material property, under a certain loading condition, the fracture of the component being assessed may initiate at a material region far away from the crack tip. Such a phenomenon cannot be explained by classical linear elastic fracture mechanics (LEFM), since LEFM always predicts unrealistic singular stresses at the crack tip, which inevitably leads to the conclusion that failure must start at the crack apex. On the other hand, since the material microstructural features are not modelled explicitly, LEFM usually fails to capture the fracture behavior of components containing short cracks (Askes and Susmel, 2014) (i.e. the situation whereby the investigated crack length is of the same order of magnitude as the material characteristic length), in which the detrimental effect of the crack becomes insignificant and the fracture is more inclined to initiate at other regions away from the crack tip (Taylor, 2011). In this condition, new methods should be developed to predict and explain these special fracture modes.

Examination of the state of the art shows that, currently, two linear elastic approaches are available to solve the aforementioned shortcomings of LEFM and can be used to verify the existence of this special interior fracture mode also in cracked/notched components. The first approach is the so-called gradient elasticity (see Askes and Aifantis, 2011, for a broad overview). This approach introduces a material-dependent microscopic characteristic length parameter incorporating higher-order spatial gradients into the constitutive equation

of the material which, thus, can remove singularities from the crack tip fields. Therefore, the crack tip stress can directly be used to assess the actual failure condition of the component (Askes et al., 2013). Further, since the underlying material microstructural characteristic are considered in the material constitutive equations, gradient elasticity can also be used to capture accurately the behavior of cracks having different lengths (Susmel et al., 2013).

Another approach that can be used to avoid the ambiguities of stress singularities is the Theory of Critical Distances (TCD) (Taylor, 2007). The fundamental ideas on which the TCD is based can be dated back to the pioneering works of Neuber (1958) and Peterson (1959). These methods were then reformulated by Taylor (1999, 2007, 2008) to make them suitable for addressing different structural integrity problems. The basic principle of this linear elastic method is to use an effective stress calculated at a certain distance away from the crack tip, or by averaging over a line, area or volume around the crack tip (depending on the material microstructural characteristics which will be described in detail later) to assess the failure of the cracked component. Thus, the linear elastic integrity assessment of a cracked component can directly be performed, with this removing the problem of singular stresses at the crack tip. On the other hand, since this type of approach implicitly accounts for the material microstructure via a material-depended length scale parameter, it can be used to evaluate the failure of components with complex stress concentration features (such as notches, cracks and corners) under different scale dimensions (Askes et al., 2013). In recent years, the TCD has been extended to other ambits of the structural integrity discipline. The theory was shown to be successful in estimating the static strength of notched/cracked brittle and quasi-brittle material (such as PMMA, cement, rocks) (Taylor, 2004; Susmel and Taylor, 2008a; Cicero et al., 2012, 2014) as well as of notched/cracked ductile material subjected to uniaxial (Susmel and Taylor, 2008b; Madrazo et al., 2012) and multiaxial static loading (Li et al., 2016; Susmel and Taylor, 2010a, 2010b). It is clear, then,

that the TCD allows accurate and robust analysis of the complex fracture behaviour of cracked-bodies to be performed in a very accurate way.

This paper aims to use the linear-elastic TCD to analyze a particular interior fracture mode. Such a fracture mode has been observed in a recent work conducted by the present authors (Li et al., 2016), where the failure of a flat plate specimen, having double symmetrical notches at the gauge section and subjected to a mixed tensile-shear loading, was observed to initiate at the central region, rather than at the stress raiser tips, which cannot be explained and estimated by LEFM. Here, analytical formulae (using standard beam theory as well as the TCD) are derived to estimate the critical loading condition of a classical double-cracked flat plate specimen subjected to mixed mode I / mode II loading. Subsequently, an expression for the critical loading angle required to trigger the interior failure mode is obtained by imposing the failure conditions at the crack tip and in the central region of the specimen to be valid simultaneously. The influence of the crack length, specimen geometry and material parameters on the critical loading angle for central failure condition is then discussed in detail. Finally, in order to verify the validity of the proposed central fracture prediction formulae, linear-elastic stress analysis for two double-cracked specimens made of different materials and having different loading angles is conducted using the finite element software ABAQUS, where the validation of the proposed analytical formulae are verified by comparing the results obtained from both the theoretical formulae and the numerical simulations.

2. Theoretical considerations

2.1 Geometry and loading of the double-cracked flat plate specimen

The geometry of the double-cracked flat plate specimen investigated in this paper is shown in Fig.1(a), where the parameters $2b$ and t refer to the width and thickness of the plate, respectively. Two symmetrical cracks are assumed to be located in the gauge section

of the plate with the length of both cracks being equal to a. The investigated specimen can be treated as a plane stress or plane strain problem according to the variation of the plate thickness. In order to create a mixed tensile-shear stress state (i.e. mixed mode I and mode II loading state) at the gauge section, uniaxial in-plane tension load F, with a certain angle β between the specimen axis and the force direction, is applied at both ends of the specimen (see Fig.1(a)). Such a loading condition is equivalent to applying simultaneously uniaxial tension load F_N and in-plane shear forces F_S ($F_N=Fcos\beta$, $F_S=sin\beta$) at both ends of the gauge section (see Fig.1(b)). Further, a two-dimensional Cartesian coordinate system X-Y and a polar coordinate system r-θ are used, with their origins being located at the crack tip (see Fig.1(b)).

2.2 Procedure and basic assumptions

The object of this paper is to verify the existence of the special condition in which the crack initiates at the central region (i.e. the central material point with a coordinate (b-a,0) as shown in Fig.1(b)), rather than the crack tip, of the double-cracked flat plate specimen under in-plane mixed mode I / mode II loading and derive the corresponding analytical formulae for such a special condition. The specific steps of the derivation are as follows:

(1) The linear elastic stress field in the central region of the double-cracked specimen under mixed modes loading is obtained by using elastic beam theory. Correspondingly, the failure condition at the central region of the specimen can be obtained.

(2) Next, the linear elastic stress field at the crack tip of the specimen under mixed mode loading is obtained by using classical elastic continuum mechanics (Lazzarin and Tovo, 1996). The failure condition at the crack tip is then derived by applying the TCD to these results.

(3) By equating the failure conditions from steps (1) and (2), an analytical expression for the critical condition in which the fracture occurred at both the crack tip and the central

region can be obtained. This formula can be used to determine the geometry and loading angles required for satisfying the special central failure condition.

(4) Finally, two types of double-cracked flat plate specimens, having different loading angles, have been analysed using finite element software ABAQUS. The accuracy of the proposed analytical formula is checked by comparing the results obtained from the theoretical formulae and the numerical simulations.

In addition, the following assumptions need to be made prior to the actual derivations:

(1) The material is taken to be isotropic and elastic. No flaws or voids are considered.

(2) The line of action of the uniaxial force applied at both ends of the specimen crosses the central point of the gauge section. Thus, the gauge section is only subjected to an axial force F_N and shear force F_S, without bending moment.

(3) The crack length a is much smaller than the half-width of the specimen b, i.e. $a<<b$. This assumption ensures that the stress fields at the crack tip and the center of the specimen do not interfere with each other.

(4) As usual, different equivalent stress measures may be appropriate for different materials (e.g. maximum principal stress for brittle materials and Tresca or von Mises' stress for ductile materials). Thus, the maximum principal stress σ_1 (for brittle material) and von Mises' stress $\bar{\sigma}$ (for ductile material) are adopted as the stress indices to derive the critical loading formulae for specimens made of different materials.

2.3 Failure condition at central region of the double-cracked flat plate specimen

According to the classical elastic beam theory, for a double-cracked flat plate specimen subjected to in-plane uniaxial tension load F_N and pure shear load F_S (as shown in Fig.1(b)), the distributed normal stress σ_n and the shear stress τ along the cross-section containing the two cracks (i.e. plane $y=0$) can be expressed as:

$$\sigma_n = \frac{F_N}{2(b-a)t} \tag{1}$$

$$\tau = \frac{F_s}{2I}\left(\frac{[2(b-a)]^2}{4} - x_1^2\right) = \frac{3F_S x(2b-2a-x)}{4t(b-a)^3} \tag{2}$$

where, I is the inertia moment of the cross-section containing the two cracks ($I = \frac{1}{12}t(2b-2a)^3$), whereas $x_1 = b-a-x$ is a conversion coordinate.

Accordingly, the maximum principal stress σ_1 and von Mises' stress $\bar{\sigma}$ at the central cross-section ($y=0$) can be obtained by using the following conversion relationships:

$$\sigma_1 = \frac{1}{2}\sigma_n + \frac{1}{2}\sqrt{\sigma_n^2 + 4\tau^2} = \frac{F_N}{4(b-a)t} + \frac{1}{(2b-2a)^3 t}\sqrt{144x^2\left(b-a-\frac{x}{2}\right)^2 F_S^2 + (2b-2a)^4 F_N^2} \tag{3}$$

$$\bar{\sigma} = \sqrt{\sigma_n^2 + 3\tau^2} = \sqrt{\frac{432x^2\left(b-a-\frac{x}{2}\right)^2 F_S^2 + (2b-2a)^4 F_N^2}{t^2(2b-2a)^6}} \tag{4}$$

From Eqs.(3-4) the maximum principal stress and von Mises' stress have their maximum at the central point of the cross-section (i.e. the point having coordinates ($b-a$,0) as shown in Fig.1(b)):

$$\sigma_{1,center} = \sigma_1(x = b-a) = \frac{F_N + \sqrt{9F_S^2 + F_N^2}}{4(b-a)t} \tag{5}$$

$$\bar{\sigma}_{center} = \bar{\sigma}(x = b-a) = \frac{\sqrt{4F_N^2 + 27F_S^2}}{4(b-a)t} \tag{6}$$

The critical failure condition can be determined by using the relevant material failure criteria, which are assumed to be expressed in terms of material ultimate tensile strength σ_{UTS}:

$$\sigma_{1,center} = \sigma_{UTS} \tag{7}$$

$$\bar{\sigma}_{center} = \sigma_{UTS} \tag{8}$$

2.4 Linear-elastic stress field at the crack tip

In order to determine the critical failure condition at the crack tip, the linear elastic stress field at the crack tip is required. Many early expressions for the linear elastic stress field at the crack tip are available, including those by Inglis (1913), Westergaard (1939) and Williams (1957). However, considering that the research results in this study can be extended to other more general notched-specimens (will be discussed in Section 4), a general closed-form solution for determining the linear elastic stress field at the tip of a V-shaped notch with an opening angle equal to 2α (as shown in Fig.2) proposed by Lazzarin and Tovo (1996) is adopted here. This analytical solution can be used to determine the linear-elastic stress field at the tip of both the V-notch and a crack (the case where the opening angle $\alpha=0$). According to the results in this research, the stress field in the vicinity of the V-notch shown in Fig. 2 can be represented as the sum of the stress fields due to modes I and II loading, respectively, where the polar stress components at the tip of the V-notch under mode I loading can be expressed as

$$
\begin{bmatrix} \sigma_\theta \\ \sigma_r \\ \tau_{r\theta} \end{bmatrix} = \frac{1}{\sqrt{2\pi}} \frac{r^{\lambda_1-1} K_I}{(1+\lambda_1)+\chi_1(1-\lambda_1)} \left[\begin{Bmatrix} (1+\lambda_1)\cos(1-\lambda_1)\theta \\ (3-\lambda_1)\cos(1-\lambda_1)\theta \\ (1-\lambda_1)\sin(1-\lambda_1)\theta \end{Bmatrix} + \chi_1(1-\lambda_1)\begin{Bmatrix} \cos(1+\lambda_1)\theta \\ -\cos(1+\lambda_1)\theta \\ \sin(1+\lambda_1)\theta \end{Bmatrix} \right] \quad (9)
$$

whereas the stress components at the tip of the V-notch under mode II loading can be written as

$$
\begin{bmatrix} \sigma_\theta \\ \sigma_r \\ \tau_{r\theta} \end{bmatrix} = \frac{1}{\sqrt{2\pi}} \frac{r^{\lambda_2-1} K_{II}}{(1-\lambda_2)+\chi_2(1+\lambda_2)} \left[\begin{Bmatrix} -(1+\lambda_2)\sin(1-\lambda_2)\theta \\ -(3-\lambda_2)\sin(1-\lambda_2)\theta \\ (1-\lambda_2)\cos(1-\lambda_2)\theta \end{Bmatrix} + \chi_2(1+\lambda_2)\begin{Bmatrix} -\sin(1+\lambda_2)\theta \\ \sin(1+\lambda_2)\theta \\ \cos(1+\lambda_2)\theta \end{Bmatrix} \right] \quad (10)
$$

In Eqs.(9-10), K_I and K_{II} are the mode I and II stress intensity factors, respectively; σ_θ, σ_r, $\tau_{r\theta}$ are the normal and shear stress components in the polar coordinate system; λ_i, χ_i (i=1, 2) are two parameters which are functions of the opening angle, α. According to the work

conducted by Lazzarin and Tovo (1996), the values for parameter λ_i ($\lambda_i > 0$) can be obtained as the minimum eigenvalue of the following equations:

$$\sin(\lambda_1 q\pi) + \lambda_1 \sin(q\pi) = 0 \qquad \text{Mode I loading (11)}$$

$$\sin(\lambda_2 q\pi) - \lambda_2 \sin(q\pi) = 0 \qquad \text{Mode II loading (12)}$$

whereas parameter χ_i can be obtained from

$$\chi_i = -\frac{\sin\left[(1-\lambda_i)q\pi/2\right]}{\sin\left[(1+\lambda_i)q\pi/2\right]} \qquad (13)$$

Parameter q in Eq.(13) is a coefficient which is used to establish the geometrical relationship between the Cartesian coordinate system and the auxiliary curve coordinate system as defined by Lazzarin and Tovo (1996), which has the following geometrical relations with opening angle 2α:

$$q = 2 - \frac{2\alpha}{\pi} \qquad (14)$$

The crack investigated in this study is a special case of V-notch with an opening angle $2\alpha=0$. In this case, the crack tip stress field parameters are $q=2$, $\lambda_1 = \lambda_2 = 0.5$, $\chi_1 = \chi_2 = 1.0$. Then, by substituting these parameters into Eq.(9) and (10), the stress components at the crack tip under mode I and mode II loading on the plane crossing the two cracks ($\theta=0$) can be derived as:

$$\sigma_{xI} = \frac{K_I x^{-\frac{1}{2}}}{\sqrt{2\pi}}, \quad \sigma_{yI} = \frac{K_I x^{-\frac{1}{2}}}{\sqrt{2\pi}}, \quad \tau_{xyI} = 0 \qquad \text{mode I loading (15)}$$

$$\sigma_{xII} = 0, \quad \sigma_{yII} = 0, \quad \tau_{xyII} = \frac{K_{II} x^{-\frac{1}{2}}}{\sqrt{2\pi}} \qquad \text{mode II loading (16)}$$

Then, by applying the equivalent conversions to Eqs.(15-16), the stress field at the crack tip expressed in terms of maximum principal stress $\sigma_{1,crack}$ and von Mises' stress $\bar{\sigma}_{crack}$ can

be obtained in terms of stress intensity factors K_I and K_{II} as

$$\sigma_{1,crack} = \frac{1}{2}[(\sigma_{xI} + \sigma_{xII}) + (\sigma_{yI} + \sigma_{yII})] + \frac{1}{2}\sqrt{[(\sigma_{xI} + \sigma_{xII}) - (\sigma_{yI} + \sigma_{yII})]^2 + 4(\tau_{xyI} + \tau_{xyII})^2} = \frac{K_I + K_{II}}{\sqrt{2\pi}} x^{-\frac{1}{2}}$$

(17)

$$\bar{\sigma}_{crack} = \sqrt{(\sigma_{xI} + \sigma_{xII})^2 + (\sigma_{yI} + \sigma_{yII})^2 - (\sigma_{xI} + \sigma_{xII})(\sigma_{yI} + \sigma_{yII}) + 3(\tau_{xyI} + \tau_{xyII})^2} = \frac{\sqrt{K_I^2 + 3K_{II}^2}}{\sqrt{2\pi}} x^{-\frac{1}{2}} \quad (18)$$

In general, the mode I and mode II stress intensity factors, i.e. K_I and K_{II}, can be expressed as functions of the remote normal stress, the shear stress and the geometry correction factor $G(a/b)$:

$$K_I = \sigma_N \sqrt{\pi a} G$$

(19)

$$K_{II} = \tau \sqrt{\pi a} G$$

(20)

Then, the general forms for the maximum principal stress, $\sigma_{1,crack}$, and von Mises' stress, $\bar{\sigma}_{crack}$, at the crack tip on the plane crossing the two cracks can be obtained by substituting Eqs.(19-20) into Eqs.(17-18):

$$\sigma_{1,crack}(x) = \frac{\sqrt{2a}G}{4(b-a)tx^{\frac{1}{2}}} F_N + \frac{3\sqrt{2a}Gx^{\frac{1}{2}}\left(b-a-\frac{x}{2}\right)}{4(b-a)^3 t} F_S$$

(21)

$$\bar{\sigma}_{crack}(x) = \left\{ \frac{aG^2}{8(b-a)^2 t^2 x} F_N^2 + \frac{27aG^2\left(b-a-\frac{x}{2}\right)^2}{8(b-a)^6 t^2} F_S^2 \right\}^{1/2}$$

(22)

Eqs.(21-22) are the analytical solutions for the stress fields at the crack tip of the double-cracked flat plate expressed in terms of maximum principal stress $\sigma_{1,crack}$ and von Mises' stress $\bar{\sigma}_{crack}$. As it can be seen from Eqs.(21-22), both the maximum principal stress and von Mises' stress at the crack tip can be expressed as polynomial terms of power

functions of *x*, which depend on the geometry (*b*, *t*, *G*), the crack length (*a*) and the applied external loads (*F_N* and *F_S*). When *x* tends to 0 (i.e. the tip of the crack), both the maximum principal stress and von Mises' stress tend to infinity (stress singularity phenomenon caused as described by LEFM), with this holding true irrespective of the magnitude of the external loads being applied to the specimen. This stress singularity precludes the direct use of the stress value at the crack tip to determine the actual failure condition.

2.5 Failure conditions at the crack tip

As discussed in the introduction, the Theory of Critical Distances (TCD) (Taylor, 2007) is a local linear elastic failure analysis method, which can be used to overcome the ambiguities due to crack-tip stress singularities. According to the integration domains being adopted for determining the effective stress, in two-dimensional analysis the different formalizations of the TCD are the Point Method (PM), the Line Method (LM) and the Area Method (AM). In this study, the PM in the TCD is used to derive the critical failure condition at the crack tip of the double-cracked flat plate specimen being investigated, where the principle of the PM is illustrated in Fig.3.

The PM (see Fig.3(b)) is the simplest version of the TCD. The PM postulates that, for a cracked specimen subjected to arbitrary external loads (see Fig.3(a)), the failure of the cracked specimen being assessed is assumed to occur when the effective stress, σ_{eff}, determined at a distance $L/2$ from the crack tip on the straight line experiencing the maximum stress gradient, equals the material inherent strength σ_0, i.e.:

$$\sigma_{eff} = \sigma\left(\theta = 0, r = L/2\right) = \sigma_0 \tag{23}$$

In Eqs.(23), σ is the equivalent linear-elastic stress at the crack tip, which can be calculated according to one of the classical hypotheses (e.g. Von Mises, Tresca, maximum principal stress criterion, etc.), whereas, L and σ_0 are the so-called material critical distance and inherent strength, respectively. Both L and σ_0 are material constants, which are related to

the ductility and strength of the material being assessed (Taylor, 2007). The most accurate way to determine these two material properties is to conduct experiments on samples containing, at least, two different geometrical features (Li et al., 2016; Taylor, 2007; Susmel and Taylor, 2008b, 2010b). Fig.4 schematically depicts the specific steps for determining L and σ_0, where the two stress-distance curves are plotted, in the incipient failure condition, in terms of the adopted equivalent stress obtained by testing a sharp and blunt notch, respectively. According to the PM, the coordinates of the point at which these two curves intersect each other directly gives the values of both L and σ_0.

According to the PM (Eq.(23)), the critical failure condition at the crack tip expressed in terms of maximum principal stress, $\sigma_{1,eff}$, and von Mises' stress, $\bar{\sigma}_{eff}$, can be obtained as:

$$\sigma_{1,eff} = \sigma_{1,crack}\left(x = \frac{L}{2}\right) = \frac{\sqrt{a}G}{2(b-a)tL^{\frac{1}{2}}}F_N + \frac{3\sqrt{a}GL^{\frac{1}{2}}\left(b-a-\dfrac{L}{4}\right)}{4(b-a)^3 t}F_S = \sigma_0 \tag{24}$$

$$\bar{\sigma}_{eff} = \bar{\sigma}_{crack}\left(x = \frac{L}{2}\right) = \left[\frac{aG^2 F_N^2}{4(b-a)^2 t^2 L} + \frac{27aLG^2\left(b-a-\dfrac{L}{4}\right)^2 F_S^2}{16(b-a)^6 t^2}\right]^{\frac{1}{2}} = \sigma_0 \tag{25}$$

2.6 Analytical formulae for central failure condition

In Sections 2.3-2.5, the analytical solutions of the failure conditions at both the central region and the crack tip of the double-cracked flat plate specimen have been derived – see Eqs.(7-8) and Eqs.(24-25). In order to obtain the special fracture mode in which the crack initiates at the center of the specimen rather than the crack tip, we need Eqs.(7-8) as well as Eqs.(24-25) being not satisfied at the same time.

Further, it should be noted that, according to the basic principle of the TCD, the value of the ultimate tensile strength σ_{UTS} is always less than (for ductile materials) or equal to (for classic brittle materials) the material's inherent strength σ_0 (Taylor, 2007; Ameri et al. 2015;

Susmel and Taylor, 2010b; Li et al., 2016; Louks et al., 2016):

$$\sigma_{UTS} \leq \sigma_0 \tag{26}$$

Correspondingly, the special central failure mode can be obtained as long as the effective stress σ_{eff}, determined by the TCD at the crack tip, is lower than the peak stress value σ_{center} at the central point of the specimen during the entire loading process:

$$\sigma_{1,eff} \leq \sigma_{1,center} = \sigma_{UTS} \leq \sigma_0 \qquad \text{for brittle material} \tag{27}$$

$$\bar{\sigma}_{eff} \leq \bar{\sigma}_{center} = \sigma_{UTS} \leq \sigma_0 \qquad \text{for ductile material} \tag{28}$$

In order to explain the meaning of Eqs.(27-28), Fig.5 shows an example of the maximum principal stress distribution at both the crack tip and the central region of the double-cracked flat plate specimen having a crack length $a=2$ mm and a half-width $b=40$ mm under a unit tensile-shear load (i.e. $F_N=1$ kN and $F_S=1$ kN). The black solid line in the figure is the stress distribution at the central region of the specimen determined by Eq.(3), whereas the red solid line is the maximum principal stress distribution at the crack tip determined by Eq.(21). It should be noted that since the crack investigated in this study is a small crack with the crack length a being much smaller than the specimen half-width b (a<<b), the value of geometry correction factor $G(a/b)$ maintains at the well-known 1.12 with little variation. Thus, $G=1.12$ is adopted here and in the following derivations.

Then, by substituting Eqs.(5-6) and Eqs.(24-25) into Eqs.(27-28) with factor G being equal to 1.12, the analytical formula for the special central failure mode can be obtained in terms of both the maximum principal stress and the von Mises' stress.

For brittle material:

$$\sigma_{1,eff} = \frac{1.12\sqrt{a}}{2(b-a)tL^{\frac{1}{2}}}F_N + \frac{3.36\sqrt{a}L^{\frac{1}{2}}\left(b-a-\dfrac{L}{4}\right)}{4(b-a)^3 t}F_S \leq \sigma_{1,center} = \frac{F_N + \sqrt{9F_S^2 + F_N^2}}{4(b-a)t} \tag{29}$$

For ductile material:

13

$$\bar{\sigma}_{eff} = \left[\frac{(1.12)^2 \, aF_N^2}{4(b-a)^2 \, t^2 L} + \frac{27 \cdot (1.12)^2 \, aL\left(b-a-\dfrac{L}{4}\right)^2 F_S^2}{16(b-a)^6 t^2} \right]^{\frac{1}{2}} \leq \bar{\sigma}_{center} = \frac{\sqrt{4F_N^2 + 27F_S^2}}{4(b-a)t} \qquad (30)$$

Since the angle between the uniaxial tension load, F_N, and the shear force, F_S, is defined as β (see Fig.1(a)), namely $\tan\beta = F_S/F_N$, Eq.(29) can be elaborated as

$$\tan\beta = \frac{F_S}{F_N} \geq -\frac{C_3\left(9C_1C_3 + \sqrt{9C_1^2C_2^2 + C_2^4 - 9C_2^2C_3^2}\right)}{C_2^3 - 9C_2C_3^2} - \frac{C_1}{C_2} \qquad (31)$$

where $C_1 = \left(2.24\sqrt{a} - \sqrt{L}\right)(b-a)^2$, $C_2 = 3.36\sqrt{a}L\left(b-a-\dfrac{L}{4}\right)$, $C_3 = (b-a)^2\sqrt{L}$

Similarly, Eq.(30) can be simplified as

$$\tan\beta = \frac{F_S}{F_N} \geq \left\{ \frac{4\left(L - a(1.12)^2\right)(b-a)^4}{27\left[(1.12)^2 \, aL^2\left(b-a-\dfrac{L}{4}\right)^2 - (b-a)^4 L\right]} \right\}^{1/2} \qquad (32)$$

Eqs.(31-32) are the formulae of the central failure condition for the double-cracked flat plate specimen. They indicate that, for a double-cracked specimen with a given specimen geometry (*a*, *b*) and material length scale (*L*), the fracture of the double-cracked flat plate specimen being investigated will initiate at the central point of cross-section rather than the crack tip when the specimen loading angle *β* exceeds a certain value. This result directly proves the existence of interior failure for a cracked-component from a theoretical point of view, which is obviously different from the prediction result given by the classical LEFM.

Further, it should be noted that, despite the critical loading angle formulae derived above, an ultimate load is needed for triggering the central failure condition of the specimen. According to section 2.3, the critical ultimate load F_u for triggering the central failure condition of the double-cracked flat plate specimen can be easily obtained by substituting the Eqs.(5-6) into Eqs.(7-8):

For brittle material:

$$F_u = \frac{4(b-a)t\sigma_{UTS}}{\cos\beta_c + \sqrt{1+8\sin^2\beta_c}} \qquad (33)$$

For ductile material:

$$F_u = \frac{4(b-a)t\sigma_{UTS}}{\sqrt{4+23\sin^2\beta_c}} \qquad (34)$$

where β_c is the corresponding critical loading angle determined by Eq.(31) and (32).

2.7 Influence of the specimen geometry and material properties on the critical loading angle

According to Eqs.(31-32), the critical loading angle required for the special central failure condition of the double-cracked flat plate specimen can be expressed as a function of crack length a, specimen half-width b and the material length parameter L. In order to investigate the influence of geometrical parameters a, b and the material parameter L on the critical loading angle β, nine double-cracked specimen configurations with different crack length a and half-width b were investigated. Three types of crack length, i.e. a=2 mm, 5 mm and 10 mm, and three types of crack length to specimen half-width ratio a/b, i.e. a/b=1/10, 1/15 and 1/20, are adopted.

Fig.6 shows the relationship between critical loading angle β and critical distance L for the investigated nine specimen configurations calculated according to Eq.(32). As it can be seen, both the crack length, a, and the material parameter, L, have obvious influences on the critical loading angle, β. Their effects can be summarized as follows:

(1) the required critical loading angle β for satisfying the central failure condition of the double-cracked flat plate specimen increases as material critical distance L decreases;

(2) the crack length has a significant effect on the critical loading angle, β: under the same value of L (i.e. for the same adopted material), the critical loading angle β increases

with the increase of the crack length a;

(3) the crack length, a, also has a significant influence on the critical distance, L, required for the central failure condition: under the same loading angle β, the value of L for central failure condition increases as the crack length increases;

(4) for configurations with identical crack length, the ratio a/b has insignificant effect on both the critical loading angle, β, and the critical distance, L.

In the meantime, in order to further investigate the influence of geometrical and material's parameters on β-L/a function curves, the abscissa, L, in Eq.(32) and Fig.6 was normalized (i.e. by dividing L by a). Correspondingly, a critical loading angle equation expressed in terms of the L to a ratio can be obtained as follow

$$\tan\beta=\frac{F_S}{F_N}\geq\left\{\frac{4\left(\frac{L}{a}-(1.12)^2\right)\left(\frac{b}{a}-1\right)^4}{27\left[(1.12)^2\left(\frac{L}{a}\right)^2\left(\frac{b}{a}-\frac{L}{4a}-1\right)^2-\frac{L}{a}\left(\frac{b}{a}-1\right)^4\right]}\right\}^{1/2} \tag{35}$$

where the relationship between the critical loading angle, β, and ratio L/a for the investigated nine specimen configurations are shown in Fig.7.

As it can be seen in Fig.7, the following important aspects need to be highlighted:

(1) the crack length, a, and ratio a/b has no obvious effects on the β-L/a function. It is interesting to see that, the β-L/a function curves for specimens having different crack lengths and crack-length to specimen half-width ratio are basically coincident.

(2) For the investigated nine configurations in this study, Eq.(32) is only valid for the regime when ratio $L/a<1.255$. According to Taylor (2011), ratio L/a, which is also called normalised defect size, can be used to assess the detrimental effect of the pre-existing crack on the overall behavior of the component: the crack basically has no detrimental effect on the overall strength of the specimen when the value of crack length a is far lower than that of the material's critical distance L. Conversely, the crack is damaging and will

reduce the overall strength of the specimen when the crack length is far larger than the material critical distance, L, where, under such circumstances, the detrimental effect of the crack can be quantitatively assessed by using LEFM. Obviously, Eq.(32) predicts the failure of the specimen containing the crack with obvious detrimental effect. This result proves from a theoretical point of the view that failure of a component with the overall behavior controlled by the local behavior at the crack tip may initiate at other material regions far away from the crack tip.

(3) According to Eq.(35), the limit condition of the critical loading angle Eq.(35) is $\beta=0°$, where, under such circumstances, $L/a=G^2=1.255$. This result indicates that geometry correction factor $G(a/b)$ determines the upper boundary of the L to a ratio required for triggering the central fracture condition in the double-cracked flat plate specimens.

3. Numerical verification of the central failure formulae

This section aims to verify numerically the validity and accuracy of the linear elastic stress field formulae (3-4) for the central region, formulae (21-22) for the crack tip and the proposed central failure formulae (31-32) for the double-cracked flat plate specimen being assessed. For this purpose, two types of double-cracked flat plate specimens, made of different materials, were adopted (see Fig.8). The geometric and material parameters of the two double-cracked specimens are taken as follows:

(1) $a=2$ mm, $b=40$ mm ($a/b=1/20$), $t=2$ mm, $L=0.609$ mm;

(2) $a=2$ mm, $b=40$ mm ($a/b=1/20$), $t=2$ mm, $L=2.081$ mm.

According to Eq.(31) and Eq.(32), the critical loading angles for the central failure of the above two specimens are $\beta=45°$ and $\beta=10°$, respectively. Thus, the included angles of the investigated first and second specimen are set to be 45° and 10°, respectively - see Fig.8(a-b). For convenience, the above two specimens will be referred as Specimen-45 and Specimen-10 in what follows.

The linear-elastic stress fields of these two specimens were post-processed using FE software ABAQUS/Standard, assuming a linear-elastic behavior. Two-dimensional plane FE models (see Figs.9-10) were solved to determine the relevant linear-elastic stress fields. In order to obtain accurate stress fields, the mesh density in the vicinity of the crack tip of the specimen was gradually increased, resulting in elements having a size of the order of 0.01 mm. A uniaxial tension load, F, was applied at the top edge of the specimen, whereas the bottom edge of the specimen was fully fixed.

Figs.11-12 show the stress distributions, under 1 kN, in terms of maximum principal stress and von Mises' stress for the two double-cracked flat plate specimens under consideration. As it can be seen, obvious stress concentrations occur at the crack tips of the two specimens. On the contrary, compared with the stress field at the crack tip, the stress magnitude in the central region of the two specimens is relatively low.

In order to verify the adopted stress distribution formulae at both the crack tip and the center of the specimen, the stress distribution results on the cross-section across the two cracks of the two specimens are extracted. Figs.13-14 show the stress results at both the crack tip and the central region of specimen-45 and specimen-10 obtained from the analytical formulae and the FE analysis, where the black solid lines denote the stress fields at crack tip calculated by Eqs.(21-22); the blue solid lines denote the stress distributions at center of the specimen calculated by Eqs.(3-4); and the red dash lines denote the results obtained from the FE analysis.

As it can be observed in Figs.13-14, for the investigated two different materials, the stress distribution formulae (3-4) and (21-22) can successfully predict the linear elastic stress fields at both the central region and the crack tip region of the double-cracked specimens. The stress distribution curves predicted by the analytical formulae (blue and black solid lines) agree with the numerical simulation results (red dash lines) fairly well for

the two investigated regions. Further, in order to quantify the accuracy of the expression (3-4) and (21-22), the stress value at the central point of the specimen and the material point at a distance of $L/2$ away from the crack tip were extracted, respectively. The errors of formulas (3-4) and (21-22) are calculated according to the following equations:

$$\Delta_{center} = \frac{\sigma_{T,center} - \sigma_{FEA,center}}{\sigma_{T,center}} \tag{36}$$

$$\Delta_{crack} = \frac{\sigma_{T,crack} - \sigma_{FEA,crack}}{\sigma_{T,crack}} \tag{37}$$

where, Δ_{center} and Δ_{crack} denote the calculated errors of the stress field formulas (3-4) and (21-22); $\sigma_{T,center}$ and $\sigma_{FEA,center}$ are the stress values at the central point of the specimen calculated via the analytical formulae and numerical simulation, respectively; whereas, the $\sigma_{T,crack}$ and the $\sigma_{FEA,crack}$ are the stress values at the point with a distance $L/2$ away from the crack tip calculated via the analytical formulae and the numerical simulation, respectively.

Table 1 lists the prediction errors of the formula 3-4 and 21-22. As it can be seen from the Table, compared with the numerical simulation results, the errors of the adopted four analytical formulae are within 7%, which indicates that the adopted stress field formulae have high-level accuracy.

Further, in order to verify the validity of expressions (31-32), i.e. the critical central failure condition formulae, the stress values, obtained from the FE analysis, at both the central point and the point a distance $L/2$ away from the crack tip of the two specimens are compared with each other. According to the proposed formulae (31-32), under the corresponding loading angles (namely 45° and 10°investigated in this Section), the stress value at center point should be equal to that at the material point with a distance equal to $L/2$ away from the crack tip irrespective of the external loads being applied. Thus, the accuracy of the proposed critical formula can be checked by comparing the stress magnitudes at these two points.

According to this idea, Figs.13-14 show the stress values at both the central point and the material point having a distance $L/2$ away from the crack tip for the two investigated double-cracked flat plate specimens obtained from the FE analysis. As it can be observed, the stress values at these two points are very similar: for specimen-45, the magnitudes of the maximum principal stress at center and the crack tip obtained from the numerical simulation are equal to 9.72 MPa and 9.03 MPa (with a deviation of 7% between each other), respectively; whereas, for specimen-10, the magnitudes of von Mises' stress at center and at the crack tip obtained from the numerical simulation are equal to 6.76 MPa and 7.05 MPa (with a deviation of 4% between each other), respectively. These results demonstrate the validity of the proposed analytical formulae in estimating the central failure condition of the double-cracked flat plate specimen under the mixed mode I / mode II loading.

4. Discussion

4.1 Basic principle for judging the interior failure or notch failure and its extension use

In fact, according to the idea of the PM, the basic principle for judging whether a notch failure or an interior failure occurred on a specimen is to determine the position of the maximum stress point in the material region having a distance of $L/2$ away from the notch/cracked tip. According to this idea, if the maximum stress point keeps appearing at a material region far away from the notch/crack tip throughout the loading process, an interior failure will occur on the specimen. Accordingly, the ultimate strength of the specimen can be estimated by comparing the stress value obtained at this maximum stress point with the corresponding material strength limit, i.e. the σ_{UTS}. This principle holds valid for all types of notched/cracked specimen irrespective of its complexity of the geometry.

In this study, the critical central failure condition of the double-cracked flat plate

specimen being assessed is just derived based on such a basic principle. As It can be seen, under the condition of a<<b, we can easily obtain the linear elastic stress field at both the crack tip and central region of the specimen in an analytical way. Then, by ensuring the maximum stress point maintains locating at the central point of the specimen, the critical loading condition for such an interior failure mode can be obtained.

Similarly, the principle mentioned above can be also extended to derive the critical interior failure condition of other types of notched specimens by following the same procedures. However, for such types of specimens, more focus needs to be paid on how to accurately obtain the linear elastic stress field in the vicinity of the different notches. In this condition, a usage of a general approach for evaluating the stress field at the notch tip becomes more convenient. This is also why we use a general solution (i.e. Eqs.(9-14) proposed by Lazzarin and Tovo (1996)) rather than the more straightforward classic Westergaard formula to determine the stress field at the crack tip, since such a unified stress field solution can be directly extended to derive the interior failure condition of other types of notches in the future work with more generalization.

Further, it is worth to mention that the working principle above can be also extended to the specimen with a more complex geometry, e.g. a practical engineering component. Under such a circumstance, the geometric complexity of the specimen may introduce a number of stress concentrations on the surface or the interior region combining with a coupled stress fields existed on the specimen, which makes it difficult to obtain the analytical solution of the stress field. Under such a circumstance, one can still find the maximum stress point on the specimen and obtain an empirical interior failure condition formula with the aid of the numerical simulation analysis.

Finally, it should be noted that the working principle discussed above is established on the validity of the PM in the TCD. In other words, for a specific notched specimen being

assessed, what degree of the PM can be successfully applied determines the validity of such an interior failure mode determination principle. Obviously, the validity of the PM can be fully guaranteed for a crack investigated in this study, since the crack is a limit case of a notch which would introduce the highest degree of stress gradient in enough area in the vicinity of the crack tip (i.e. process zone). However, for a more general blunt notch, what extent of notch bluntness determines the invalid limit of the PM needs more works to be answered. In fact, the application range of the TCD was discussed in the Taylor's research (2007), which indicated that the application limit of the TCD depended on the relationship between the size of the process zone affected by the stress raiser and the value of material critical distance L. However, the specific details of such a topic are obviously beyond the scope of this study.

4.2 Discussion on different failure criteria applied for the crack tip and interior region

It is worth to mention that, in the process of deriving the interior critical failure condition of the double-cracked flat plate specimen, different treatments were applied for the crack tip and the central region, respectively. For the crack tip region having a high stress gradient, a LEFM based local approach (i.e. the TCD) was used to analyze the failure condition with σ_0 being as the material's strength limit. On the contrary, the central region of the specimen was treated as a plain specimen and the plain specimen's ultimate tensile strength σ_{UTS} was used as the strength limit for determining the failure condition of the region. In the author's point of view, the adoption of such a different treatment is attributed to the different overall failure mode presented by the cracked-specimen: if a notch failure occurs on the cracked-specimen, it means that the overall performance of the specimen being assessed is controlled by the local material at the crack tip. Under such a condition, a use of local approach (i.e. TCD) to determine the overall failure of the specimen is reasonable. On the contrary, if an interior failure occurs on the cracked-specimen, it means that the overall

performance of the specimen will be no longer controlled by the local material at the crack tip region. In other words, the cracked-specimen performs more like a plain specimen with its overall behavior transferred from a "local-controlled" mode to a "global-controlled" mode. Under such circumstances, the applicability of the TCD becomes invalid, since this theory is designed to specifically assess stress raisers rather than un-notched components. In this condition, the ultimate tensile stress σ_{UTS}, which is usually adopted as the strength limit for the un-notched material, should be used to determine the failure condition of the specimen.

However, there is another point of view on determining the failure condition of the cracked-specimen: since the stress magnitude at the interior material region maintains higher than that at the notch tip region throughout the loading, the interior material regions can be also treated as stress raisers, where, under such a condition, one can apply the TCD on all regions, i.e. use the σ_0 as the strength limit for all regions, to determine the critical failure condition of the specimen. The rationality of such an approach was actually discussed in our recent research (Li et al, 2016), which indicated that such an approach seemed to provide reasonable results compared with the experiment. However, attention must be paid when using this approach since no previous work in this field suggests that the internal material region can be regarded as a stress raiser and addressed by using a local failure theory, which needs further works to be answered properly.

Nonetheless, as it can be seen that, even if such an approach is used, it would not affect the validity of the critical central failure condition derived in this study, since as long as the stress magnitude at the central material region maintains larger than that at the crack tip throughout the loading (see Eq.(27-28)), one can ensure that the stress magnitude at central material region reaches the material strength limit σ_0 earlier than that at the crack tip region, which will result in an interior failure occurred on the specimen. The only difference caused by such an approach is that the ultimate load of the critical interior failure

condition will be changed since the σ_0 rather than the σ_{UTS} is used as the strength limit for the interior material region. In this condition, the ultimate load in Eqs.(33-34) would be changed as

For brittle material:

$$F_u = \frac{4(b-a)t\sigma_0}{\cos\beta_c + \sqrt{1+8\sin^2\beta_c}} \tag{38}$$

For ductile material:

$$F_u = \frac{4(b-a)t\sigma_0}{\sqrt{4+23\sin^2\beta_c}} \tag{39}$$

4.3 Size effect on the critical interior failure condition

According to the critical central failure formula (31-32) derived in this paper, the critical interior failure condition of the double-cracked specimen is influenced by an obvious specimen size effect (i.e. affected by the relationship between the overall size of the specimen, crack length and the value of L). In other words, in order to obtain the interior failure mode of the cracked-specimen made of a material having a specific value of L, how to choose an appropriate match between the specimen size, flaw size and the value of L becomes a key point.

Taking the double-cracked flat plate specimen designed for numerical validation in section 3 as an example, being same as the most material property test specimen, the overall size of the specimen and the crack length designed in this study are in an order of centimeter and millimeter, respectively. Accordingly, according to the critical loading angle formulae 31-32 and Fig.6, by using such a specimen size, the critical interior failure condition of different cracked materials with the value of L being in an order of millimeter can be easily obtained in a wide loading angle regime. However, when such a specimen size is used to obtain the interior failure condition of the cracked-material with a much

24

smaller *L* value, e.g. the material having a value of *L* being in an order of micron, the situation becomes difficult and unreasonable, since under such a circumstance, the interior failure condition of the cracked material being assessed can be only obtained by keeping the loading angle of the specimen at a very small area close to the 90 degrees (see Fig.6), which would provide a result with a very low resolution.

One method for solving the problem above is to adjust the relationship between the crack length, the overall specimen size and the value of *L*. In other words, according to formulae 31-32, the critical interior failure condition of the cracked material being assessed can be easily obtained as long as the three dimensions mentioned above are in the same order. Therefore, for a cracked material with a value of *L* being in an order of micron discussed above, the critical interior failure condition of the cracked material can be easily obtained in a wide loading angle regime as long as the overall specimen size and crack length is reduced in the level of dozens or hundreds of microns. However, such a situation would propose a new challenge for machining the specimen.

4.4 Similarity of this study with the Failure Assessment Diagram method

It is interesting to find that the contents in this study have a similarity with the Failure Assessment Diagram (FAD) method (Milne et al., 1988), which is a useful engineering tool for assessing the fracture-plastic collapse of the cracked components. In more details, the FAD method provides a simultaneous assessment on both fracture and plastic collapse on a cracked component by using two normalized parameters K_r and L_r, which are defined as

$$K_r = \frac{K_I}{K_C} \tag{40}$$

$$L_r = \frac{P}{P_L} \tag{41}$$

where K_I is the stress intensity factor, K_C is the corresponding material fracture toughness measured by the stress intensity factor (e.g., K_{IC}, K_{JC}, etc.), P is the applied load on the cracked component, P_L is the plastic collapse load of the component. According to the idea of the FAD, the parameter K_r is used to evaluate the resistance of the component against the fracture caused by the flaws, whereas the L_r is used to evaluate the resistance of the component against the plastic collapse. Therefore, the overall resistance of the cracked component can be assessed through a series of coordinates (K_r, L_r), which constitutes a line, i.e. the so-called Failure Assessment Line (FAL), for determining the resistance limit of the component. Under such a circumstance, if an assessment point (K_r, L_r), obtained from a cracked component is located between the FAL and the K_r-L_r coordinates axes, the component can be considered to be safe. Otherwise, a failure would occur on the cracked component being assessed.

According to the idea of the FAD, the integrity assessment on the cracked specimen conducted in this study can be performed in a similar way: i.e. using two newly defined normalized parameters σ_r and F_r to assess the notch failure and interior failure occurred on the cracked specimen, where the parameters σ_r and F_r are defined as:

$$\sigma_r = \frac{\sigma_{eff}}{\sigma_0} \tag{42}$$

$$F_r = \frac{F}{F_u} \tag{43}$$

where σ_{eff} is the effective stress used in the TCD (see Eq.(23)), σ_0 is material's inherent strength, F is the applied load on the cracked component, F_u is the ultimate load for the interior failure of the specimen (see Eqs.(33-34)). In this way, similar to the principle of the FAD, the newly defined parameter σ_r, which is established based on the PM, can be used to evaluate the resistance of the component against the fracture caused by the flaws and the parameter F_r can be used to evaluate the resistance of the component against the

interior failure. In this way, for different cracked/notched specimens, a new type of σ_r-F_r diagram can be established on the basis of the TCD to assess both the notch failure and interior failure of the specimens.

In fact, according to the results in this study, a direct relationship can be established between the PM in the TCD and the parameter K_r used in the FAD method under mode I loading condition. In more details, according to Eqs.(17-18) and Eq.(23), a connection between the effective stress σ_{eff} and the stress intensity K_I can be established under mode I loading:

$$\sigma_{eff} = \frac{K_I}{\sqrt{\pi L}} \tag{44}$$

Meanwhile, the inherent strength σ_0 in the TCD has the following relationship with the material's fracture toughness K_c (Taylor, 2007):

$$L = \frac{1}{\pi} \left(\frac{K_C}{\sigma_0} \right)^2 \tag{45}$$

namely

$$\sigma_0 = \frac{K_C}{\sqrt{\pi L}} \tag{46}$$

Then by substituting Eqs.(44) and (46) into Eq.(42), one can find that the newly defined parameter σ_r is actually equal to the parameter K_r in the FAD:

$$\sigma_r = K_r \tag{47}$$

This result is very interesting since it provides a new version of the FAD for assessing the integrity of cracked/notched specimen considering the advantages of the TCD. However, it should be noted, the relationship between the σ_r and K_r above is only limited to the mode I loading condition. For an in-plane mixed mode loading, a direct relationship between σ_0 and K_{mc}, i.e. the fracture toughness considering the mode II loading effect, is missing. Nonetheless, as it can be seen that the newly derived σ_r-F_r diagram can work well for the

cracked-specimen under the mixed-mode loading conditions, which provides a new tool for assessing the integrity of the cracked/notched specimens.

4.5 Suggestions for experimental validation

Obviously, the theoretical results in this study would benefit from a further experimental validation. However, compared with the theoretical deduction, more practical factors need to be considered in the experimental validation to ensure the accurate acquisition of the interior failure mode being assessed, where more cares should be paid on the choice of an appropriate test material, an accurate calibration of material's properties in the TCD and a reasonable design on the specimen geometry. These works will be considered in our follow-up research.

5. Conclusions

This paper uses the linear elastic Theory of Critical Distances, LEFM and standard beam theory to derive a failure condition of a special central fracture mode occurring in classical double-cracked flat plate specimens subjected to mixed mode I and mode II loading. The influence of the crack length, specimen geometry and material parameters on the critical loading angle for such a central fracture mode is fully investigated. In addition, linear elastic stress analyses were conducted on two double-cracked specimens made of different materials and having different loading angles using finite element software ABAQUS/Standard. The proposed analytical formulae were verified by comparing the results obtained from both the theoretical formulae and the numerical simulations. The main conclusions in this study can be summarized as follows:

(1) The results in this study demonstrate the possibility of interior fracture mode on the cracked-component from a theoretical point of view. According to the results in this paper, for the classical double-cracked flat plate specimen with a given geometry and material property, under a certain in-plane loading angle, fracture in a double-cracked flat plate

specimen would start at the central point, not at the crack tips.

(2) The material's critical distance L and crack length a have a significant effect on the critical loading angle of the central failure condition of the double-cracked flat plate specimen. On one hand, for the specimens containing the same crack length, the critical loading angle required for the central fracture mode decreases with the increase of the material's critical distance. On the other hand, when the investigated material is identical (i.e. having the same value of critical distance L), the critical loading angle for central fracture mode of the specimen increases with the increase of the crack length.

(3) For specimen configurations with identical crack length, the crack-length to specimen half-width ratio a/b has insignificant effects on the critical loading angle β for the central fracture mode.

(4) The results in this study provide a reference for derivation of the analytical formula of the interior failure mode for other types of cracked/notched specimens.

(5) The results in this study would benefit from further experimental validations.

Acknowledgements

Reference

Ameri, A.A.H., Davison, J.B., Susmel, L., 2015. On the use of linear-elastic local stresses to design load-carrying fillet-welded steel joints against static loading. Eng. Fract. Mech. 136, 38-57.

Askes, H., Aifantis, E., 2011. Gradient elasticity in statics and dynamics: An overview of formulations, length scale identification procedures, finite element implementations and new results. Int. J. Solids Struct. 48, 1962-1990.

Askes, H., Livieri, P., Susmel, L., Taylor, D., Tovo, R., 2013. Intrinsic material length, Theory of Critical Distances and Gradient Mechanics: analogies and differences in processing linear-elastic crack tip stress fields. Fatigue Fract. Eng. M. 36(1),39-55.

Askes, H., Susmel, L., 2014. Understanding cracked materials: is Linear Elastic Fracture Mechanics obsolete?. Fatigue Fract. Eng. M. 38, 154-160.

Cicero, S., Madrazo, V., Carrascal, I.A., 2012. Analysis of notch effect in PMMA using the Theory of Critical Distances. Eng. Fract. Mech. 86, 56-72.

Cicero, S., García, T., Castro, J., Madrazo, V., Andrés, D., 2014. Analysis of notch effect on the fracture behaviour of granite and limestone: An approach from the Theory of Critical Distances. Eng. Geol. 177, 1-9.

Inglis, C.E., 1913. Stresses in a Plate Due to the Presence of Cracks and Sharp Corners. Transactions of the Institute of Naval Architects. 55, 219-241

Lazzarin, P., Tovo, R., 1996. A unified approach to the evaluation of linear elastic stress fields in the neighborhood of cracks and notches. INT. J. Fracture. 78, 3-19.

Li, W., Susmel, L., Askes, H., Liao, F., Zhou, T., 2016. Assessing the integrity of steel structural components with stress raisers using the Theory of Critical Distances. Eng. Fail. Anal. 70, 73-89.

Louks, R., Askes, H., Susmel, L., 2016. A generalised approach to rapid finite element design of notched materials against static loading using the Theory of Critical Distances. Materials & Design. 108, 769-779.

Madrazo, V., Cicero, S., Carrascal, I.A., 2012. On the Point Method and the Line Method notch effect predictions in Al7075-T651. Eng. Fract. Mech. 79, 363-379.

Milne, I., Ainsworth, R.A., Dowling, A.R., Stewart, A.T., 1988. Assessment of the integrity of structures containing defects. INT. J. PRES. VES. PIP. 32(1-4), 3-104.

Neuber, H., 1958. Theory of notch stresses: principles for exact calculation of strength with reference to structural form and material, 2nd ed. Springer Verlag, Berlin.

Peterson, R.E., 1959. Notch sensitivity, in: Sines, G., Waisman J.L. (Eds.), Metal fatigue. McGraw Hill, New York, pp. 293-306.

Susmel, L., Taylor, D., 2008a. The theory of critical distances to predict static strength of notched brittle components subjected to mixed-mode loading. Eng. Fract. Mech. 75, 534-550.

Susmel, L., Taylor, D., 2008b. On the use of the Theory of Critical Distances to predict static failures in ductile metallic materials containing different geometrical features. Eng. Fract. Mech. 75, 4410-4421.

Susmel, L., Taylor, D., 2010a. The Theory of Critical Distances to estimate the static strength of notched samples of Al6082 loaded in combined tension and torsion. Part I: Material cracking behavior. Eng. Fract. Mech. 77, 452-469.

Susmel, L., Taylor, D., 2010b. The Theory of Critical Distances to estimate the static strength of notched samples of Al6082 loaded in combined tension and torsion. Part II: Multiaxial static assessment. Eng. Fract. Mech. 77, 470-478.

Susmel, L., Askes, H., Bennett, T., Taylor, D., 2013. Theory of Critical Distances versus Gradient Mechanics in modelling the transition from the short to long crack regime at the fatigue limit. Fatigue Fract. Eng. M. 36, 861-869.

Tada, H., Paris, P., Irwin, G., 2000. The stress analysis of cracks handbook, 3rd ed. ASME Press, New York.

Taylor, D., 1999. Geometrical effects in fatigue: a unifying theoretical model. Int. J. Fatigue. 21, 413-420.

Taylor, D., 2004. Predicting the fracture strength of ceramic materials using the theory of critical distances. Eng. Fract. Mech. 71, 2407-2416.

Taylor, D., 2007. The theory of critical distances: a new perspective in fracture mechanics. Elsevier, Oxford, UK

Taylor, D., 2008. The theory of critical distances. Eng. Fract. Mech. 75, 1696-1705.

Taylor, D., 2011. Applications of the theory of critical distances in failure analysis. Eng. Fail. Anal. 18, 543-549.

Westergaard, H.M., 1939. Bearing Pressures and Cracks. J. Appl. Mech. 6:A49-A53.

Williams, M.L., 1957. On the Stress Distribution at the Base of a Stationary Crack. J. Appl. Mech. 24,109-114.

Tables

Table 1 Prediction error of the formulae used for estimating the stress field at crack tip and central region of the specimen

Property	Stress distribution at crack tip		Stress distribution at central region	
	Formula 21 (maximum principal stress)	Formula 22 (von Mises' stress)	Formula 3 (maximum principal stress)	Formula 4 (von Mises' stress)
Error	6.71%	0.98%	0.41%	5.06%

Figures
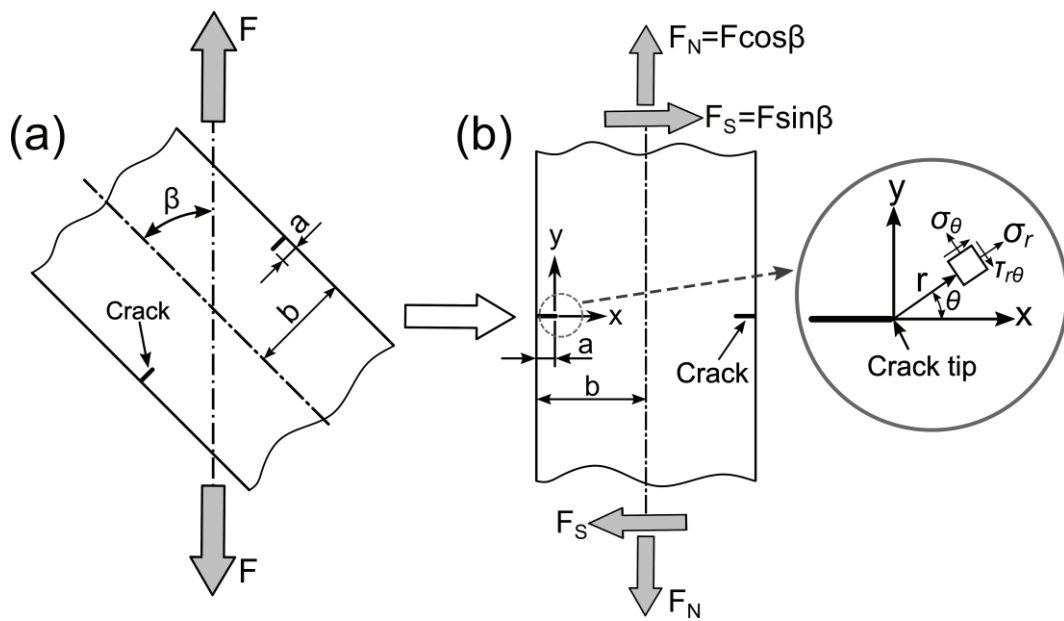
Fig.1 Geometry and loading conditions of the double-cracked flat plate specimen
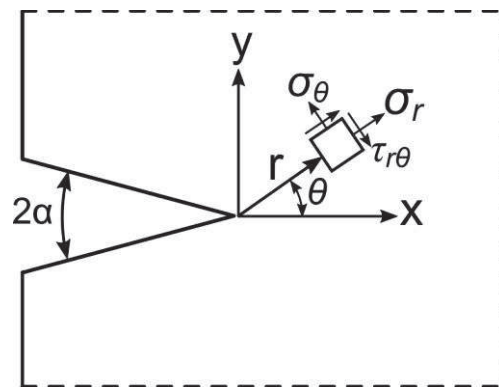
Fig.2 V-shaped notch (with an opening angle 2α) investigated by Lazzarin and Tovo (1996) and the local coordinate system located at the crack tip
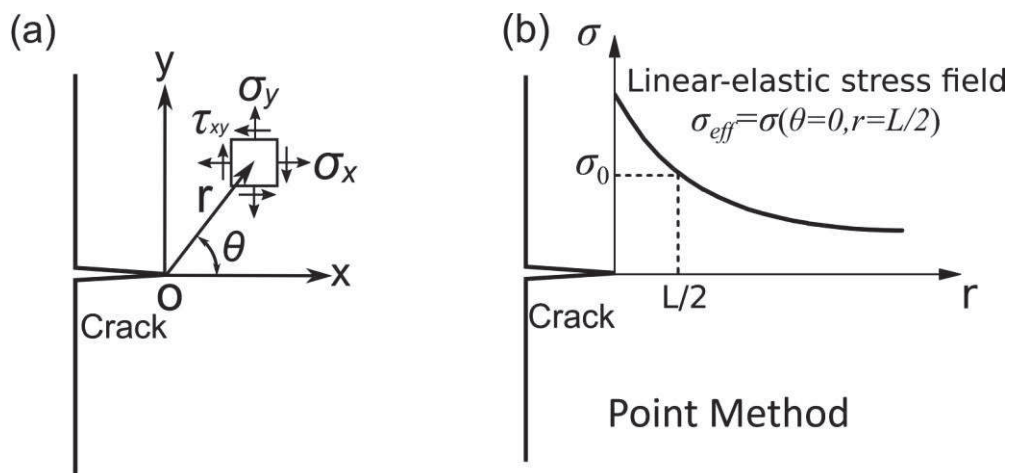
Fig.3 Local coordinate system located at the crack tip of the cracked component (a); the working principle of the Point Method (b).
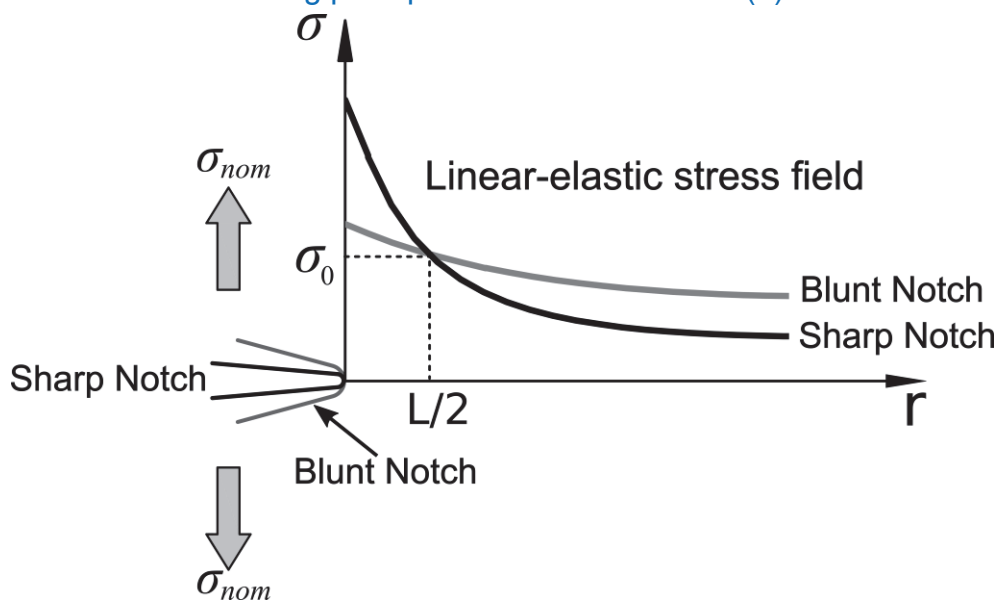
Fig.4 Determination of the material critical distance L and inherent strength σ_0 through two linear-elastic stress-distance curves generated by testing two notched specimens with different notch sharpness under nominal uniaxial loading.
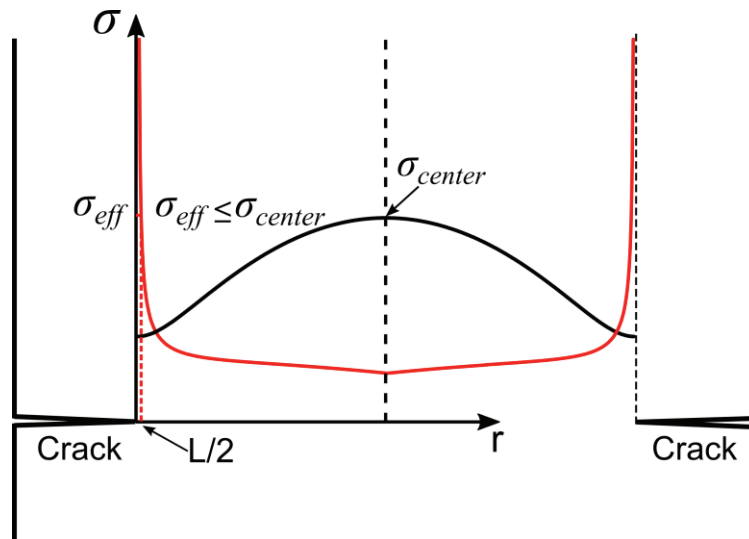
Fig.5 The critical condition for central fracture mode of the double-cracked flat plate specimen
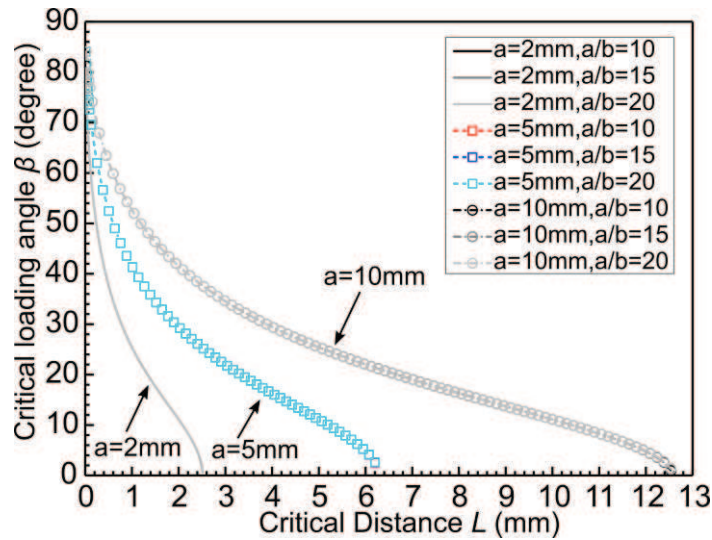
Fig.6 The relationship between the central failure critical loading angle β and the critical distance L for the investigated nine configurations
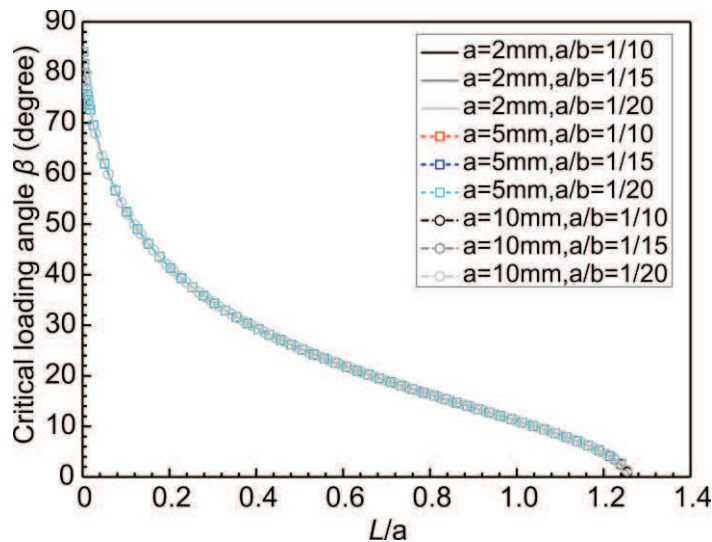
Fig.7 The relationship between the central failure critical loading angle β and the ratio L/a for the investigated nine configurations
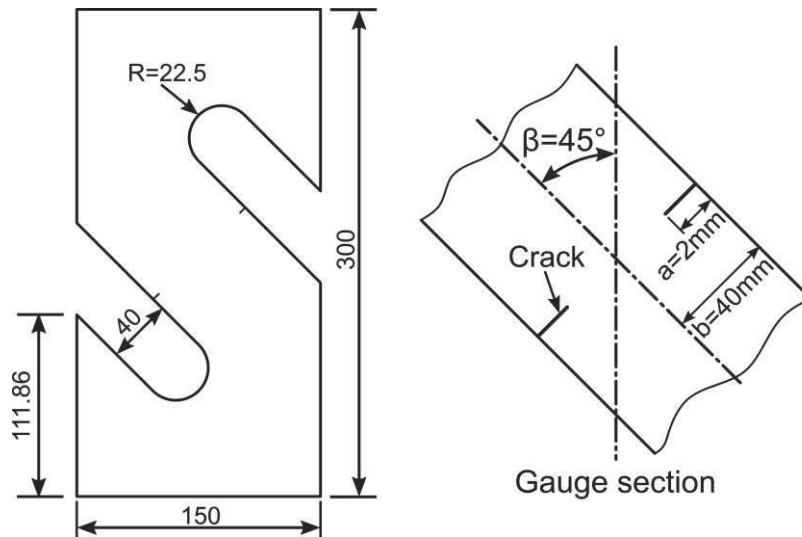
(a) The geometry of the specimen-45 (the angle between the specimen axis and loading axis is 45°)
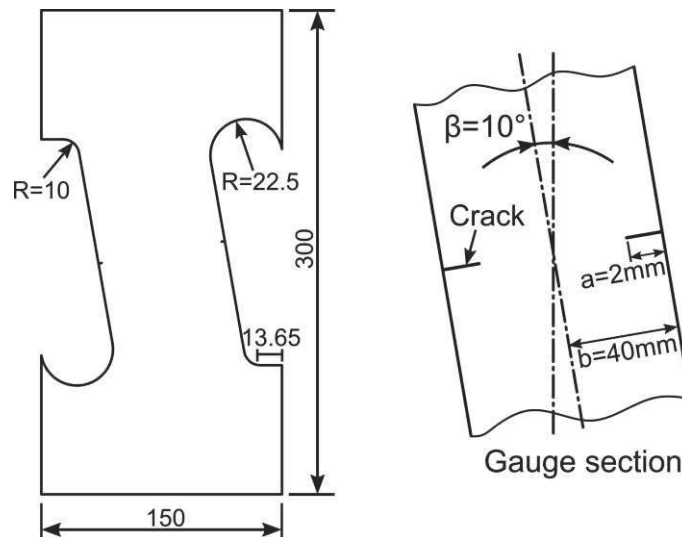
(b) The geometry of the specimen-10 (the angle between the specimen axis and loading axis is 10°)

Fig.8 The geometry of the double-cracked flat plate specimen investigated in this study (dimensions in millimeter)
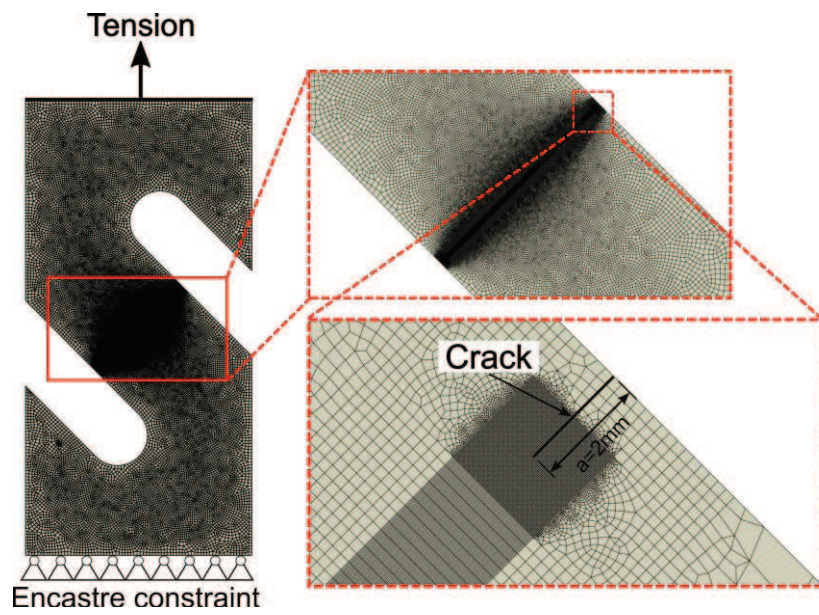
**Fig.9** The finite element model for the double-cracked flat plate specimen-45
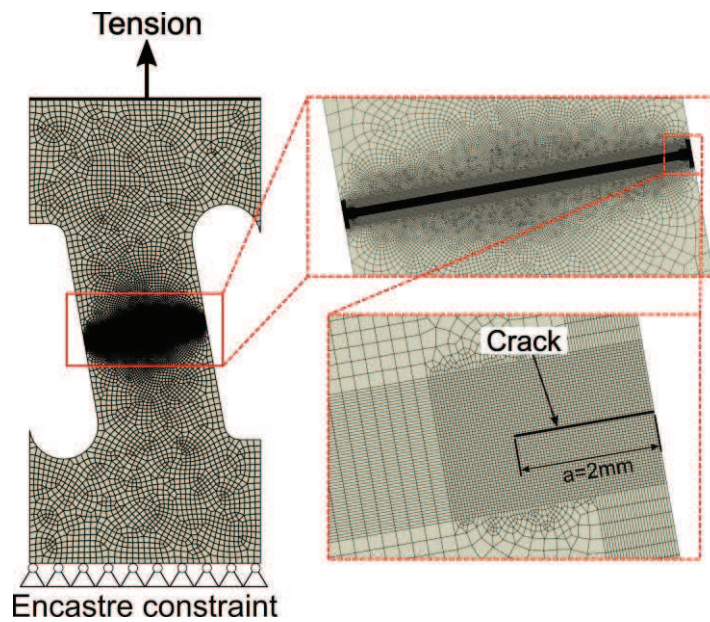
**Fig.10** The finite element model for the double-cracked flat plate specimen-10
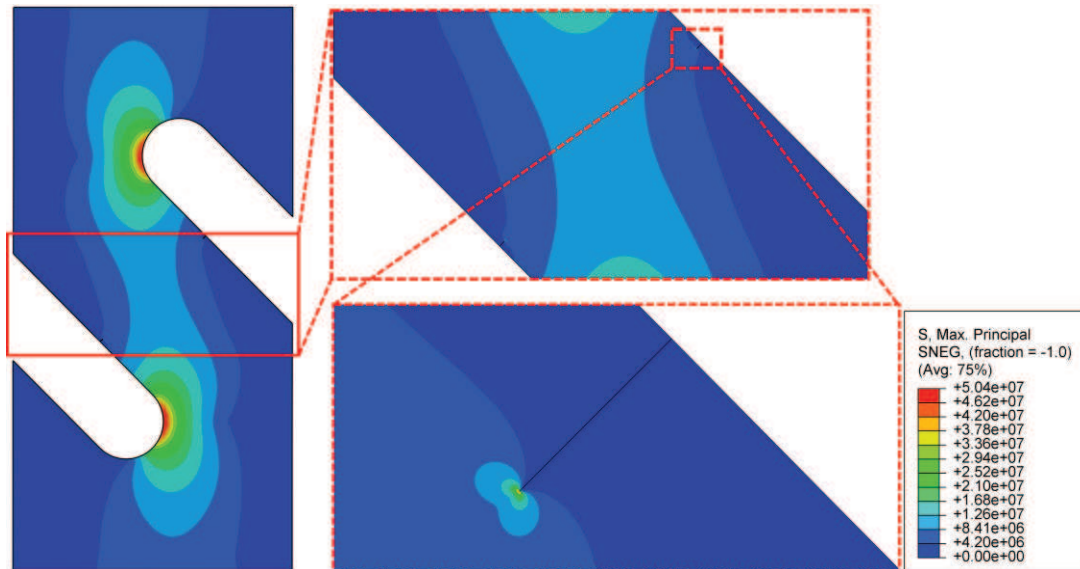
Fig.11 The maximum principal stress distribution at the gauge section and crack tip of the specimen-45 under unit tension load (1 kN)
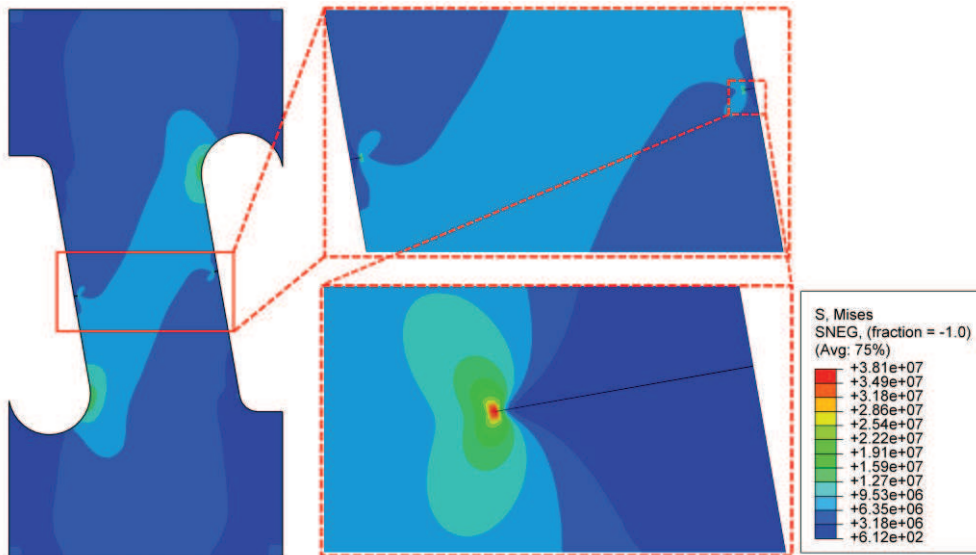

Fig.12 The von Mises' stress distribution at the gauge section and crack tip of the specimen-10 under unit tension load (1 kN)
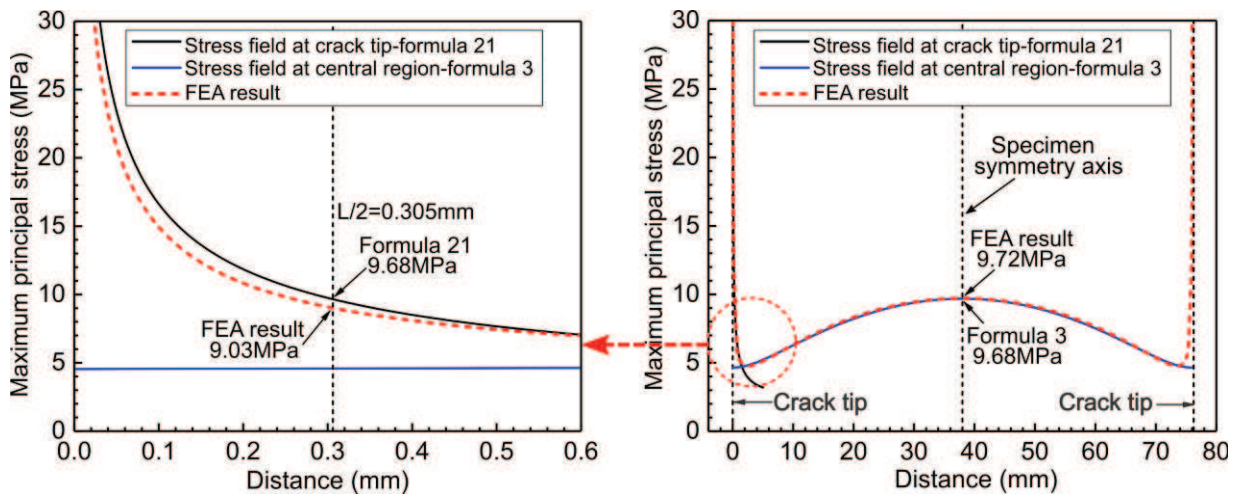
Fig.13 The maximum principal stress distribution along the cross-section of the specimen-45 under unit tension load (1 kN)
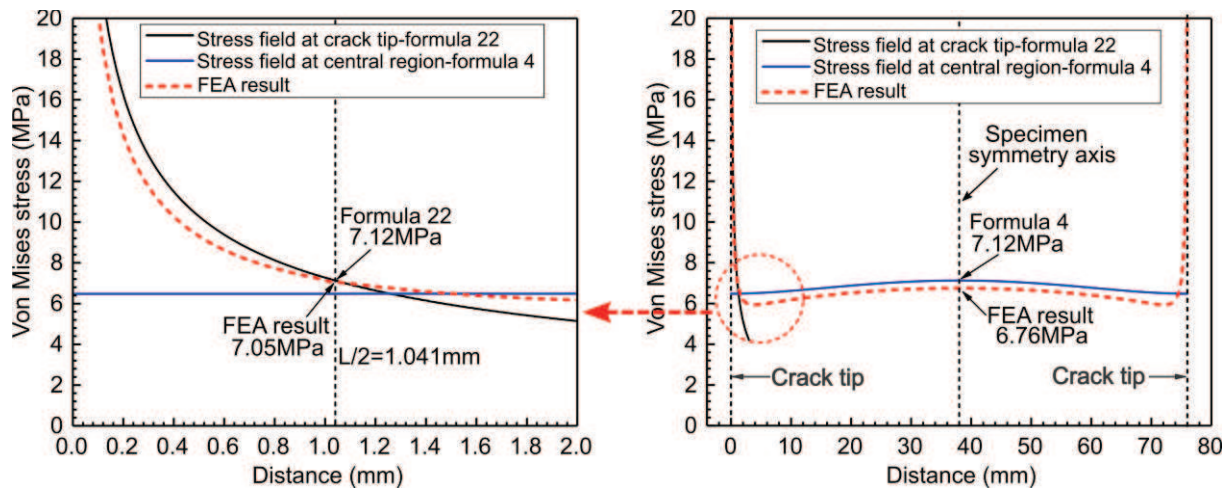

Fig.14 The von Mises' stress distribution along the cross-section of the specimen-10 under unit tension load (1 kN)